

Weierstraß-Institut
für Angewandte Analysis und Stochastik
Leibniz-Institut im Forschungsverbund Berlin e. V.

Preprint

ISSN 0946 – 8633

**Strong asymmetry of mode-locking pulses in quantum-dot
semiconductor lasers**

Mindaugas Radziunas¹, Andrei G. Vladimirov¹, Evgeny A. Viktorov²,

Gerrit Fiol³, Holger Schmeckeber³, Dieter Bimberg³

submitted: December 16, 2010

¹ Weierstrass Institute
for Applied Analysis and Stochastics
Mohrenstr. 39
10117 Berlin, Germany
E-Mail: radziuna@wias-berlin.de
vladimir@wias-berlin.de

² Optique Nonlinéaire Théorique
Université Libre de Bruxelles
Campus Plaine CP 231
B-1050 Bruxelles, Belgium
E-Mail: evviktor@ulb.ac.be

³ Institut für Festkörperphysik
Technische Universität Berlin
Hardenbergstr. 36
10623 Berlin, Germany
E-Mail: gerrit.fiol@physik.tu-berlin.de
schmeckeber@sol.physik.tu-berlin.de
bimberg@physik.tu-berlin.de

No. 1579

Berlin 2010



2010 *Mathematics Subject Classification.* 78A60, 35Q60, 35P10, 35B30.

2008 *Physics and Astronomy Classification Scheme.* 42.55.Px, 42.60.Fc, 73.63.Kv, 85.30.De, 85.35.Be.

Key words and phrases. quantum dots, semiconductor laser, saturable absorber, mode-locking, trailing edge plateaux, optical mode, mode decomposition .

Edited by
Weierstraß-Institut für Angewandte Analysis und Stochastik (WIAS)
Leibniz-Institut im Forschungsverbund Berlin e. V.
Mohrenstraße 39
10117 Berlin
Germany

Fax: +49 30 2044975
E-Mail: preprint@wias-berlin.de
World Wide Web: <http://www.wias-berlin.de/>

Abstract

We describe the formation of a strong pulse asymmetry in mode-locked quantum-dot edge-emitting two-section semiconductor lasers. A mode decomposition technique reveals the role of the superposition of different modal groups. The results of theoretical analysis are supported by experimental data.

The advantages of self-assembled quantum dot (QD) materials [1] can be exploited in multi-section mode-locked (ML) lasers which are able to generate stable high intensity picosecond and sub-picosecond pulses [2].

In this letter, we study experimentally and theoretically, strongly asymmetric ML pulses generated by an edge-emitting QD ML laser consisting of a 100 μm long saturable absorber (SA) and a 900 μm long gain section. Our particular attention is drawn to the study of the pulses having a broad trailing edge plateaux (TEP) [3]. Our theoretical analysis shows that the TEP in QD lasers arise mainly due to non-instant carrier transitions between the carrier reservoir (CR), excited state (ES) and ground state (GS) of the QDs. These multiple finite-time transitions slow-down the carrier exchange between the electrically pumped CR and the photon generating GS of QD, act as a filtering and lead to a homogenization of the carrier and photon distributions along the gain section. To reveal the role of separate optical modes in ML regimes with strongly asymmetric pulses we have performed a modal analysis [4]. The pulses with a strongly enhanced TEP can be represented as a superposition of a usual pulsating ML state formed by a large number of longitudinal modes and phase-shifted pulsations comprising only a few optical modes.

We consider a 1+1 dimensional traveling wave model describing spatial-temporal evolution of the two counter-propagating optical fields, $E^+(z, t)$ and $E^-(z, t)$, material polarization functions, $p^+(z, t)$ and $p^-(z, t)$, normalized carrier density $n_{cr}(z, t)$ within the CR, and occupation probabilities $n_{gs}(z, t)$ and $n_{es}(z, t)$ of the GS and ES of quantum dots, respectively [3].

To describe carrier exchange between the CR, GS, and ES of the QDs in the SA ($z \in [0, l_{SA}]$) and gain ($z \in [l_{SA}, L]$) sections we use the rate equations [5]:

$$\begin{aligned}
 \frac{d}{dt}n_{gs}(z, t) &= -\frac{n_{gs}}{\tau_{gs}} + 2R_{es,gs} - \frac{1}{\Theta_E}R(n_{gs}, E, p), \\
 \frac{d}{dt}n_{es}(z, t) &= -\frac{n_{es}}{\tau_{es}} - R_{es,gs} + R_{cr,es}, \\
 \frac{d}{dt}n_{cr}(z, t) &= \frac{I(z)}{\theta_I} - \frac{n_{cr}}{\tau_{cr}} - 4R_{cr,es}, \\
 R &= \Re \sum_{\nu=\pm} E^{\nu*} \left[2g'(n_{gs} - \frac{1}{2})E^\nu - \bar{g}(E^\nu - p^\nu) \right], \\
 R_{es,gs}(n_{es}, n_{gs}) &= \frac{n_{es}(1-n_{gs})}{\tau_{es \rightarrow gs}} - \frac{n_{gs}(1-n_{es})}{2\tau_{gs \rightarrow es}}, \\
 R_{cr,es}(n_{cr}, n_{es}) &= \frac{n_{cr}(1-n_{es})}{4\tau_{cr \rightarrow es}} - \frac{n_{es}}{\tau_{es \rightarrow cr}}.
 \end{aligned} \tag{1}$$

Here the function R stands for a stimulated recombination, $R_{es,gs}$ and $R_{cr,es}$ describe the carrier exchange rates between the dot's states, and τ_a^{-1} and $\tau_{a \rightarrow b}^{-1}$, $a, b \in \{gs, es, cr\}$ denote

spontaneous relaxation and transition rates between GS, ES and CR, respectively. $(1 - n_{gs})$ and $(1 - n_{es})$ represent the Pauli blocking, while factors 2 and 4 account for the degeneracy in the QD energy levels. Following Ref. [6] we assume that in the reversely biased SA section the carrier transitions from the CR to the ES can be neglected. Hence, in this section we set $\tau_{cr \rightarrow es}^{-1} = 0$ and consider only the equations for n_{gs} and n_{es} in Eq. (1).

The meaning and values of most of the laser parameters can be found in Ref. [3]. In the present letter we use the linewidth enhancement factor $\alpha_H = 2$ and the scaling factors $\Theta_I = 1.5$ A ps, $\Theta_E = 239$ W ps/m, which relate the gain section injection current $I_G = I(z)|_{z \in [l_{SA}, L]}$ and the field intensity $|E^\pm|^2$ with the scaling of n_{cr} , the QD density, the electron charge, the group velocity, and the cross-section area of the active zone. In addition, in the gain section we set $\tau_{es} = \tau_{gs} = 1$ ns, $\tau_{es \rightarrow gs} = 2$ ps, $\tau_{gs \rightarrow es} = \tau_{cr \rightarrow es} = 5$ ps, $\tau_{es \rightarrow cr} = 80$ ps. Other parameters are the same as in Ref.[3].

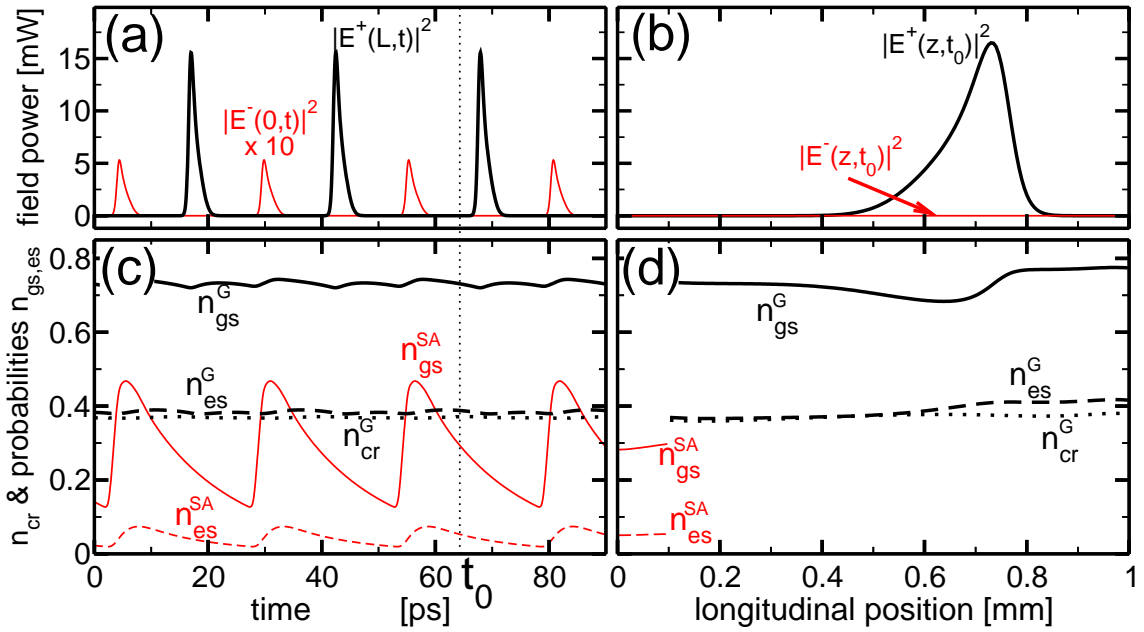


Figure 1: Typical fundamental ML pulsations ($U = -3$ V, $I_G = 40$ mA). Left: time traces of the emitted field intensities (a) and the carrier functions $n_{gs,es,cr}$ averaged over the gain and SA sections (c), respectively. Right: axial distributions of the optical fields (b) and the carrier functions (d) at the time moment t_0 .

A single light pulse traveling back and forth the laser cavity and sequentially emitted at the SA and gain section facets (see functions $|E^-(0, t)|^2$ and $|E^+(L, t)|^2$ in Fig. 1(a)) corresponds to a fundamental ML regime. A fast increase of the carrier functions n_{gs} and n_{es} in the SA section (see panel (c)) corresponds to a fast saturation of this section after the passage of a pulse.

Axial distributions of the intensities of two counter-propagating field amplitudes and carrier variables at the time moment t_0 are shown in panels (b) and (d) of Fig. 1. At this moment the power of electromagnetic field is concentrated within a pulse traveling along the laser cavity in forward direction, see the function $|E^+(z, t_0)|^2$ in Fig. 1(b). Panel (d) shows the depletion of the carriers in the gain section induced by this pulse. The strongest depletion corresponding to the largest

pulse amplification is expected to take place twice per round trip when the pulse comes close to one of the two edges of the gain section. We note, that in contrast to our previous study of a simplified two-carrier rate equation model [3], the depletion of $n_{cr}(z)$ (panel (d)) as well as the oscillation amplitude of $n_{cr}(t)$ (panel (c)) are much weaker. This is because the impact of the optical field onto the dynamics of the CR carrier density is additionally filtered by the intermediate rate equation for the ES occupation probability, which was omitted in our previous study [3].

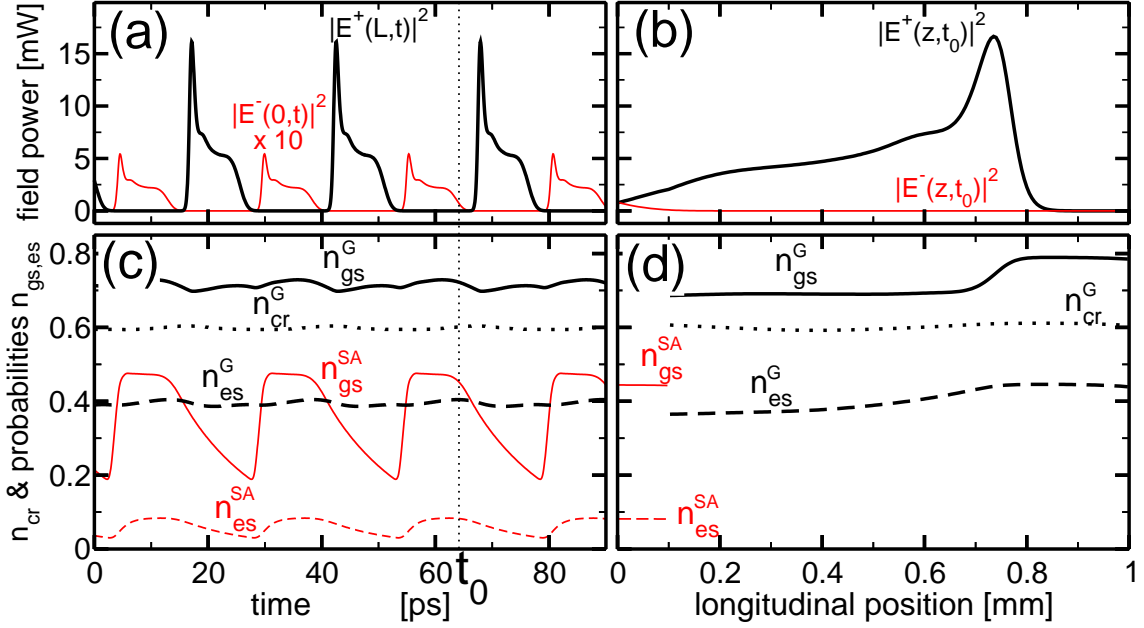


Figure 2: ML pulsation with a large plateau at the trailing edge of the pulse. Same as in Fig. 1, but for $I_G = 80\text{mA}$.

Fig. 2 represents another typical ML regime computed with injection current I_G twice as large as that used in Fig. 1. Let us emphasize the most important differences between these two ML regimes: (i) At larger injections a ML pulse has a long TEP. (ii) While the emitted pulse energy increases with the injection current, the peak intensity of the output field remains almost unchanged. (iii) Carrier density n_{cr} of the gain section increases with the injection current. The occupation probabilities n_{es} and n_{gs} which are pumped indirectly by $R_{cr,es}$ and $R_{es,gs}$ remain nearly unchanged. (iv) In the panels (c) of both figures, the growth and decay rates of n_{gs} in the SA section are similar. However, in Fig. 2 this probability has long flat maxima indicating the absorber saturation by the long TEP of the ML pulse. These maxima correspond to the plateaux of pulses emitted at the SA facet (see solid gray curves in panels (c) and (a)). The formation of strongly asymmetric pulses with TEP is unknown for the bulk or quantum well based devices, what directly confirms the role of at least one non-instant carrier transition between the CR and the GS.

In order to get a deeper understanding of the formation mechanisms of stable ML pulses with a long TEP, we have performed a modal analysis[4] of the model equations. Introducing a differ-

ential operator $H(\beta)$, we rewrite the field equations [3] in the operator form:

$$\frac{d}{dt}\Psi(z, t) = H(\beta)\Psi(z, t), \quad \Psi \stackrel{def}{=} (E^+, E^-, p^+, p^-)^T. \quad (2)$$

The field function $\Psi(z, t)$ can be decomposed into a series of instantaneous ($\beta(t)$ -dependent) modes:

$$\Psi(z, t) = \sum_k f_k(t)\Theta_k(\beta, z) \Rightarrow E^+(L, t) = \sum_k f_k(t), \quad (3)$$

where Θ_k and f_k are properly scaled eigenfunctions of the spectral problem $H(\beta)\Theta(\beta, z) = i\Omega(\beta)\Theta(\beta, z)$, and complex modal functions representing the contribution of k -th mode to the field emitted from the gain section facet, respectively. $\Re e\Omega_k$ and $\Im m\Omega_k$ give a main contribution to the rotation and damping of the modal functions [4] which can be written in the form

$$f_k(t) = f_0(t)s_k(t)e^{ik(2\pi t/T_c - \psi_k(t))}, \quad k \in \mathbf{Z}.$$

Here, $s_k(t) = |f_k/f_0|$ and $\psi_k(t)$ are real slowly varying T_c -periodic functions, where T_c is the period of ML regime close to the field round-trip time in the laser cavity. Relative phases $\psi_k(t)$ represent the phase difference between the k -th mode and the mode with the largest amplitude to which we assign the index "0". The perfect locking between several equidistant modes having equal intensities corresponds to $\psi_k(t) = \bar{\psi}(t)$ and $s_k(t) \equiv 1$. Then the relation $t/T_c = \bar{\psi}(t)/2\pi \bmod(1)$ determines the time moments when the ML pulse peaks are expected.

The shape of a ML pulse depends strongly on the relations between the amplitudes and phases of the complex modal functions. Hence, using the mode decomposition (3) the contribution of the different modes into the formation of ML pulse can be revealed.

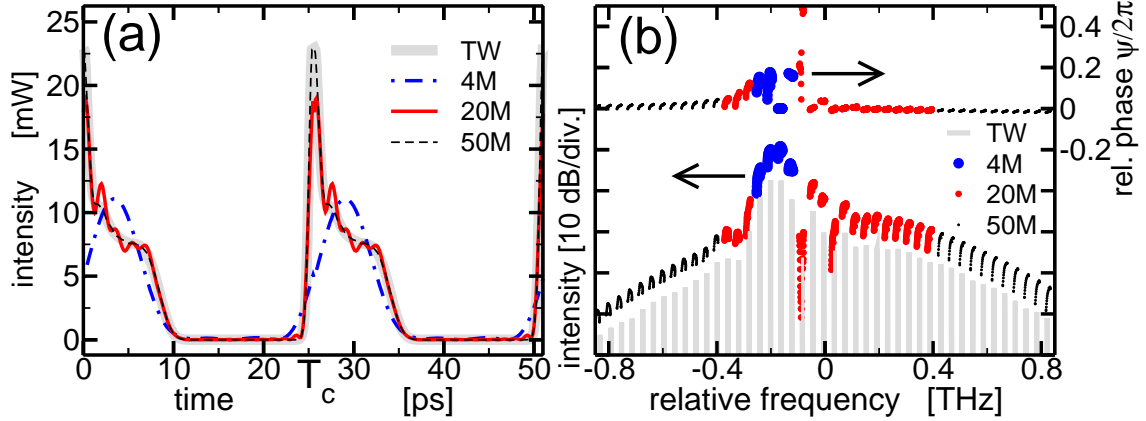


Figure 3: Modal analysis of a ML regime shown in Fig. 2. (a): Calculated time trace of the field intensity emitted at the gain section facet (thick gray curve) and its reconstruction using 50, 20 and 4 modes with largest $|f_k|$ (thin curves). (b): Bullets give a parametric representation of the modal phases $\psi_k(t)$ (above) and amplitudes $|f_k(t)|$ (below) vs. modal frequencies $\Re e\Omega_k(t)$. Optical spectrum of the emitted field is shown by solid line. Bullets of different size indicate modes used for the field reconstruction in panel (a).

A total number of 200 modes centered around the gain peak frequency have been used in the decomposition of the field function $\Psi(z, t)$, see Fig. 3. After that, a reconstruction of the electric

fields have been performed with the help of a superposition of m modes ($m = 4, 20, 50$) having largest amplitudes. We notice that the reconstruction with $m = 50$ modes gives almost perfect approximation of the original field function, while 4- and 20-mode reconstructions are not sufficient to recover the precise shape of the calculated pulse.

The comparison of field reconstructions with different numbers of modes m shows an interesting feature of ML pulses with a broad TEP. For conventional ML state an increase of the number of phase-locked modes usually leads to an increase of the pulse amplitude and a decrease of the pulse width without a significant shift of the pulse peak location. In our case, however, when increasing the number m from 4 to 50 the peak location of the reconstructed pulse shifts by 15 – 20% of the pulse repetition period T_c . This indicates that the strong asymmetry in the pulse shape appears not only due to larger amplitudes of a few most powerful central modes but also due to specific phase relations between these modes and the rest of the optical spectrum.

In Fig. 3(b), the amplitudes and relative phases of modes are shown vs their frequency. All these modes give a similar contributions to the formation of the sharp main peaks of the ML pulses located at $t \approx 0$ and $t \approx T_c$ in Fig. 3(a). Only a few most powerful modes in the central part of the optical spectrum have the phases ψ_k shifted from zero by approximately 15 – 20% of the period. These shifts correspond to the shift of the TEP from the position of the main peak, see the dash-dotted line in Fig. 3(a)). Therefore, we can conclude that TEP is formed by a few most powerful modes.

Thus, an optical field of a ML pulse with a TEP can be represented as a sum of two components: $E^+(L, t) = E_1(t) + E_2(t)$. The intensities of the components, $|E_1(t)|^2$ and $|E_2(t)|^2$, have the same periodicity T_c . While $|E_1(t)|^2$ has a form of a narrow high intensity pulse, $|E_2(t)|^2$ corresponds to a rather broad pulse with a time-shifted peak and smaller peak power.

Experimental studies of the ML pulse broadening have been performed with a ridge waveguide two section QD monolithic ML laser. The material incorporated is InGaAs forming 15 stacked layers of QDs. The device was integrated in a module comprising a fiber pigtail, a microwave port, dc contacts, and a thermoelectric cooler [7, 8].

Fig. 4 gives two different time-domain representations of the pulses measured for several injection currents I_G . The autocorrelation (AC) functions of these pulses (panel (a)) clearly show a typical increase of the pulse width with injection current. Note that for $I_G = 100\text{mA}$ the AC function has non-vanishing wings, which is typical for pulses with the intensity remaining distinguishable from zero for more then the half of the pulse repetition period.

Fig. 4(b) shows the corresponding pulses reconstructed by means of the FROG technique [9]. Similarly to our theoretic predictions, the shape of the front edge of the pulse remains nearly independent of I_G , while the pulse broadening is due to the growing trailing edge. At higher currents ($I_G = 80\text{mA}$) the formation of the TEP is visible. At even higher injections, however, the pulse reconstruction fails, since the FROG algorithm requires zero intensities at the edges of the corresponding AC functions.

In conclusion, we demonstrated numerically and experimentally, that the increase of the injection current in a monolithic two-section mode-locked QD laser leads to a formation of ML pulses with a large TEP formed by a few central modes having much larger amplitudes than the remaining ML modes.

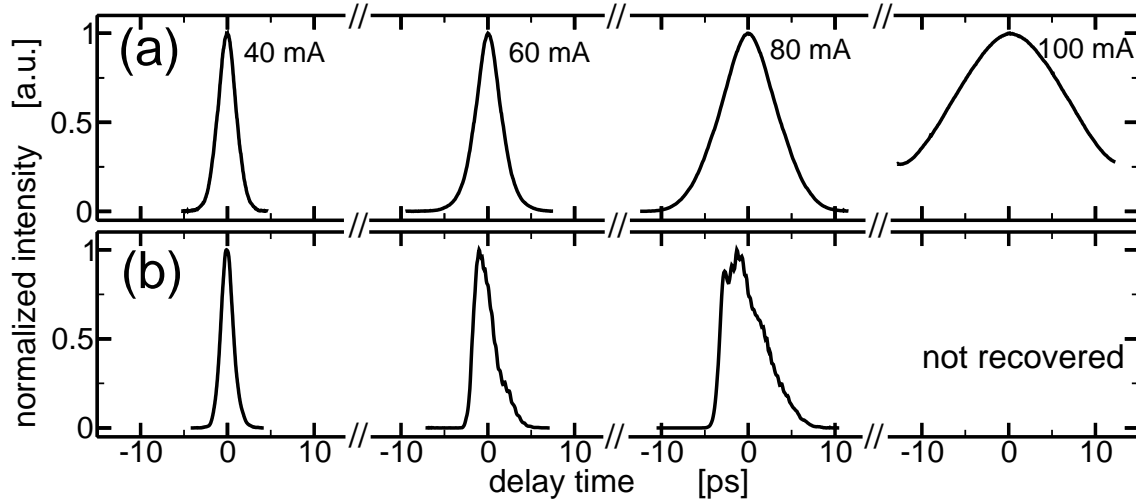


Figure 4: Experimental AC measurements (a) and reconstructed pulse shapes using FROG technique (b) at fixed voltage of the SA section and several values of the injection currents into the gain section.

The work of M. Radziunas was supported by DFG Research Center MATHEON. A. G. Vladimirov and the authors from TU Berlin acknowledge the support from SFB 787 project of the DFG. E. Viktorov is thankful to the support of Fond National de la Recherche Scientifique.

References

- [1] N. N. Ledentsov, D. Bimberg, and Z. I. Alferov, "Progress in Epitaxial Growth and Performance of Quantum Dot and Quantum Wire Lasers," *J. Lightwave Technology* **26**, 1540 (2008).
- [2] E. U. Rafailov, M. A. Cataluna, and W. Sibbett, "Mode locked quantum-dot lasers," *Nat. Photon.* **1**, 395 (2007).
- [3] M. Radziunas, A. G. Vladimirov, and E. A. Viktorov, in "Traveling wave modeling, simulation and analysis of quantum-dot mode-locked semiconductor lasers," *Proc. of SPIE*, Vol. 7720 (2010) p. 77200X.
- [4] M. Radziunas and H.-J. Wünsche, "Multisection lasers: longitudinal modes and their dynamics," in "Optoelectronic devices - advanced simulation and analysis," (Springer, New York, 2005) Chap. 5, pp. 121–150.
- [5] A. Markus, M. Rossetti, V. Calligari, D. Chek-Al-Kar, J. X. Chen, and A. Fiore, "Two-state switching and dynamics in quantum dot two-section lasers," *J. of Applied Physics* **100**, 113104 (2006).

- [6] E. A. Viktorov, T. Erneux, P. Mandel, T. Piwonski, G. Madden, J. Pulka, G. Huyet, and J. Houlihan, "Recovery time scales in a reversed-biased quantum dot absorber," *Appl. Phys. Lett.* **94**, 263502 (2009).
- [7] G. Fiol, C. Meuer, H. Schmeckeber, D. Arsenijevic, S. Liebich, M. Laemmlin, M. Kuntz, and D. Bimberg, "Quantum-dot semiconductor mode-locked lasers and amplifiers at 40 GHz," *IEEE J. Quantum Electron.* **45**, 1429 (2009).
- [8] H. Schmeckeber, G. Fiol, C. Meuer, D. Arsenijevic, and D. Bimberg, "Complete pulse characterization of quantum-dot mode-locked lasers suitable for optical communication up to 160 Gbit/s," *Optics Express* **18**, 3415 (2010).
- [9] D. J. Kane and R. Trebino, "Characterization of arbitrary femtosecond pulses using frequency-resolved optical gating," *IEEE J. Quantum Electron.* **29**, 571 (1993).